Electronic Supplementary Material (ESI) for Journal of Materials Chemistry A.

Supporting Information

High Photogeneration and Low Recombination Rate Leading to High-Performance Non-Fullerene Organic Solar Cells

Yanxian Ma§, Quanbin Liang*§, and Hongbin Wu*, Yong Cao

Institute of Polymer Optoelectronic Materials and Devices, State Key Laboratory of Luminescent Materials and Devices, South China University of Technology, Guangzhou, 510640, P. R. China.

*E-mail: liangqb@scut.edu.cn, hbwu@scut.edu.cn

§ *Y.M. and Q.L. contributed equally to this paper*

1. Experiment details

1.1 Device Fabrication.

Donor material D18 was purchased from 1-Material Inc., whereas non-fullerene acceptors (Y6, BTP-eC9, L8-BO and IT-M) were provided from Solarmer Materials, Inc.; both were used as received. The BHJ conventional device structure is ITO/PEDOT: PSS/ active layer/PDIN/Ag. Precleaned indium tin oxide (ITO)-patterned glass substrates (Nanbo Glass Inc., Shenzhen, P. R. China) were treated with O_2 plasma for 3 min before being coated with a 40 nm PEDOT:PSS (Clevios P AI4083) and baked at 150 °C for 15 min. The ITO substrates were then transferred into a glovebox filled with N_2 gas. The D18: NFA bulk heterojunction active layer, with optimized thickness around 110 nm, was prepared by spin-coating the chloroform solution of D/A blends (1/1.2 weight ratio, donor concentration is 5 mg/ml) at 2800 rpm for 1 min. A thin PDIN layer (~5 nm) was spin-coated on the active layer, followed by thermally deposition of Ag cathode (100 nm) in a vacuum chamber, and device areas of 4 mm^2 were defined by the shadow mask.

1.2 Device Characterization and measurements.

J-V Characteristics. J-V characteristics were recorded using a Keithley 2400 source meter under a 1 sun; AM 1.5G spectrum from a solar simulator (SAN-EI Inc., model: XES-40S1), solar-simulator irradiance was calibrated using a standard monocrystal silicon reference cell (Hamamatsu S1133, with KG-5 visible color filter), which was calibrated by the National Renewable Energy Laboratory (NREL).

External Quantum Efficiency. EQE was determined by an integrated system (QE-R, Enlitech Inc.). The sub-band gap EQE spectra were obtained using Fourier-transform photocurrent spectroscopy.

EL Spectroscopy. EL spectra were acquired by a spectroradiometer PR-745 (Photo Research, Inc.) or a high-sensitivity spectrometer (QE Pro or NIR Quest 512, Ocean Optics). The radiation flux of EL was determined by measuring the emitted photons in all directions through an integrated sphere by using calibrated spectrometers (QE Pro, and NIRQuest-512, Ocean Optics), under a constant current density with a Keithley 2400 source measure unit.

Transient Optoelectronic Analyses. In TPV measurement, solar cell devices were first illuminated by a halogen lamp with 100 mW/cm2illumination to reach working condition. A set of neutral optical filter were utilized to produce 0.01-1 sun illumination. Perturbed charge carriers are then generated by a 532 nm laser pulse from a Nd:YAG pulse laser (Q-smart 100 of Quantel). The TPV signals were monitored by a Tektronix DPO4014 oscilloscope with high input impedance option to achieve open-circuit condition, and the recorded transients were fitted with a mono exponential decay course to extract the lifetime of photogenerated carriers. For TPC measurement, solar cell devices were in series with a 50 Ω load resistor and voltage transient across the resistor was recorded by the oscilloscope under the same illumination and laser perturbation. The transient is translated into a current transient by Ohm's law. The photogenerated charge ΔQ by laser perturbation is the time-integrated current transient. All transient data consist of 128 voltage transient averaged together to counteract the fluctuation of laser pulse.

Fourier-transform photocurrent spectroscopy measurement. FTPS measurements using a Nicolet iS50 (Thermo Scientific) with an external detector option. Photocurrents generated from the solar cells were amplified by a low-noise current amplifier (SR570) with light modulated by the Fourier transform infrared spectroscope (FTIR).

Charge Carrier Mobilities Measurements. The hole-only devices with the structure of ITO/PEDOT:PSS/active layer/MoO_3/Al and the electron-only devices with the structure of ITO/ZnO/active layer/PDIN/Al were fabricated. The charge carrier mobility was determined by fitting the current-bias characteristics in the dark using a field-independent space charge limited current (SCLC) model following the Mott-Gurney law given by $J = \frac{9}{8}\varepsilon_0\varepsilon_r\mu\frac{V^2}{L^3}$, where J is the current density, ε_0 is the permittivity of free space, ε_r is the relative permittivity of the active layer, $\mu$is the carrier mobility, L is the film thickness of the active layer, and V is the effective voltage which is determined by subtracting the built-in voltage (V_{bi}) from the applied voltage ($V= V_{appl}-V_{bi}$).

2. Figures

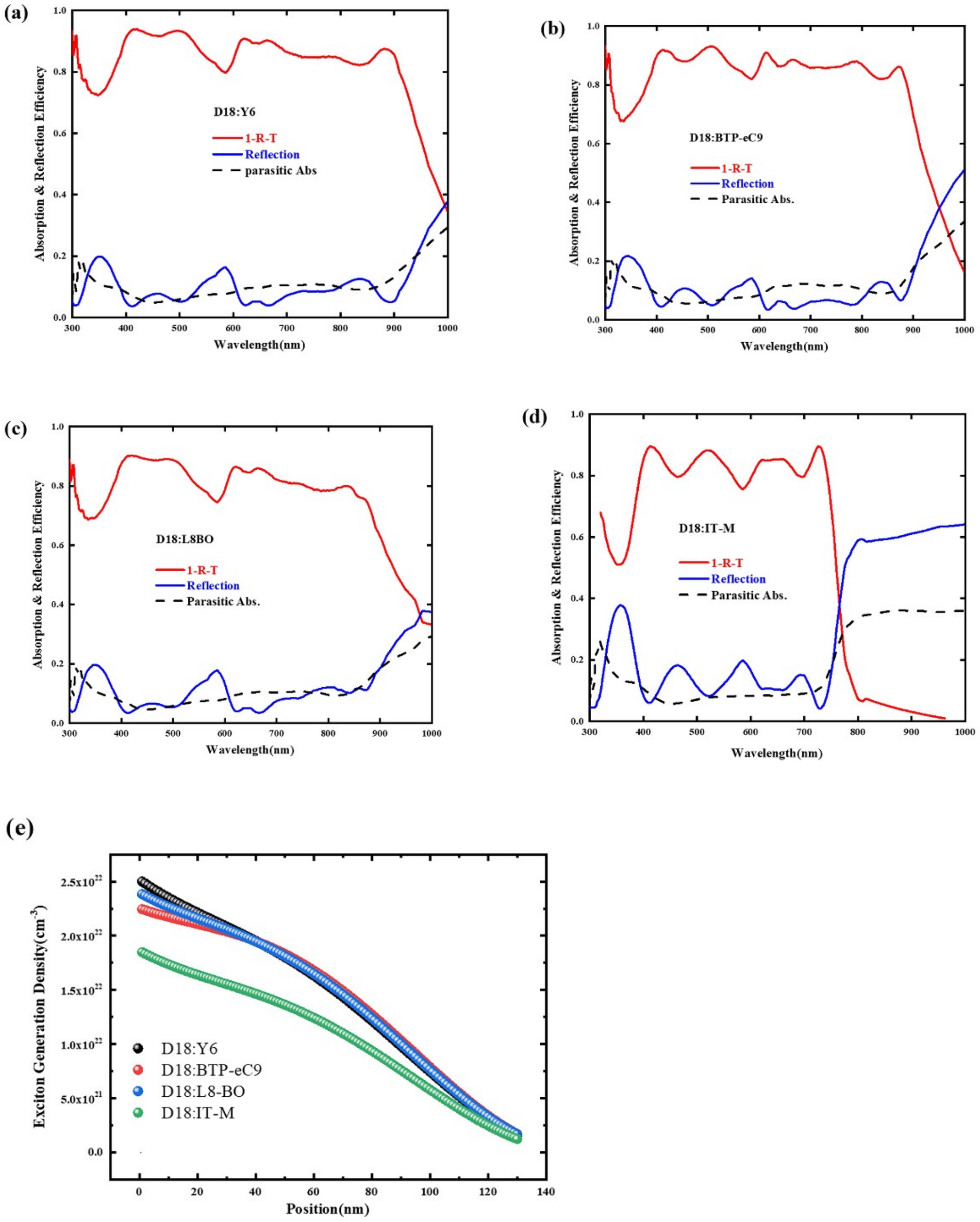

Fig. S1 (a-d) Active layer absorption efficiency (1-R-T), reflection efficiency and parasitic absorption as a function of wavelength for these four devices under AM 1.5G illumination according to simulation model. (e)Simulated exciton generation profile G_{ex} as a function of position for these four devices.

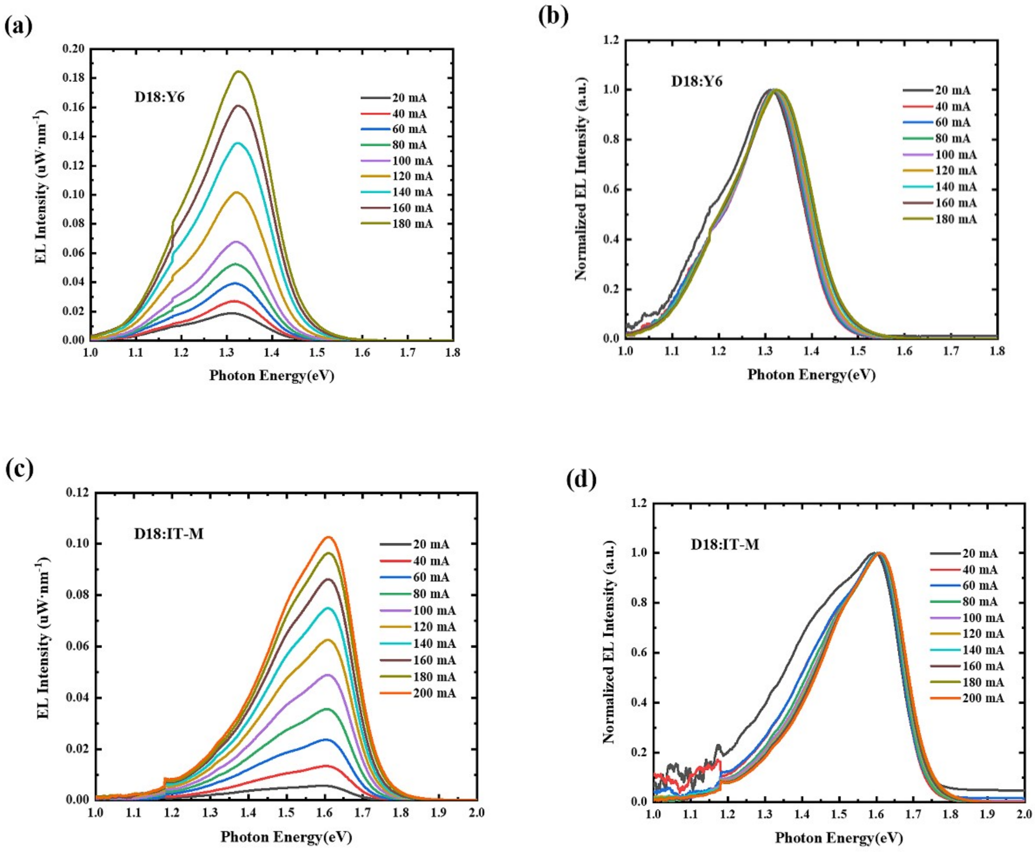

Fig. S2 Dependence of EL spectra on injection current densities (a and b) D18:Y6 device. (c and d) D18:IT-M device.

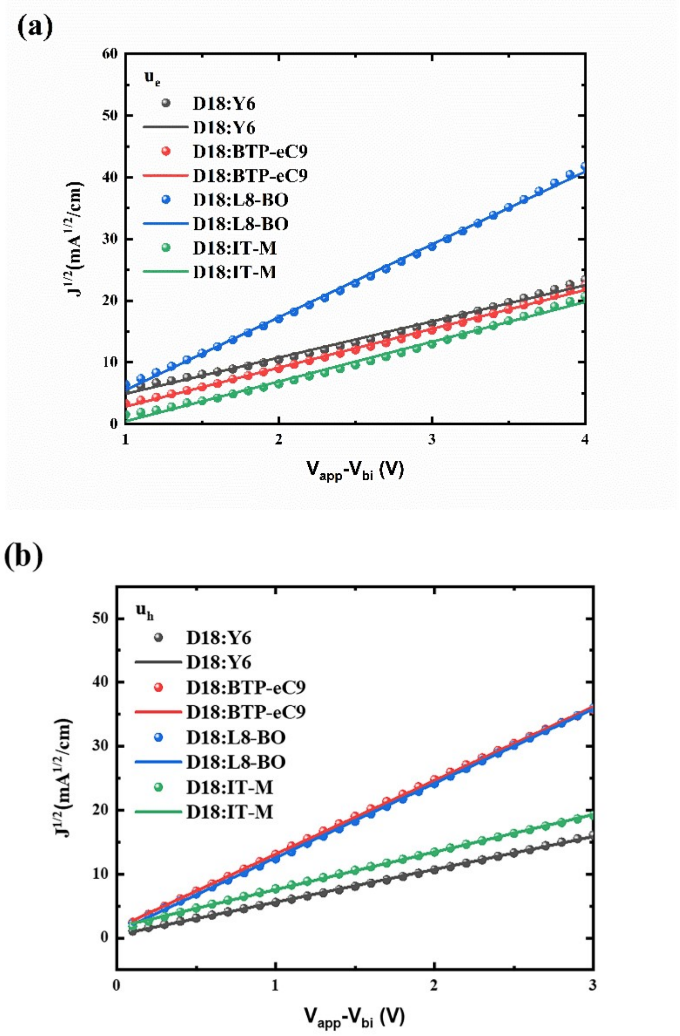

Fig. S3. Current density-voltage characteristics of D18-based electron-only (a) and hole-only (b) devices.

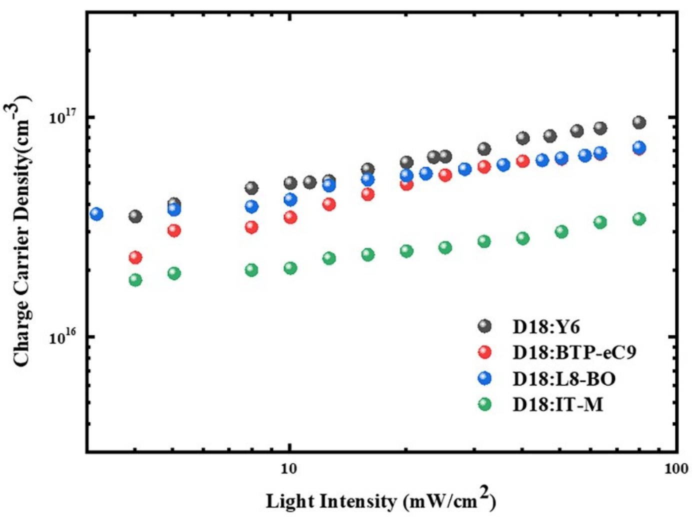

Fig. S4. Charge density measured in the device as a function of different bias light intensities.

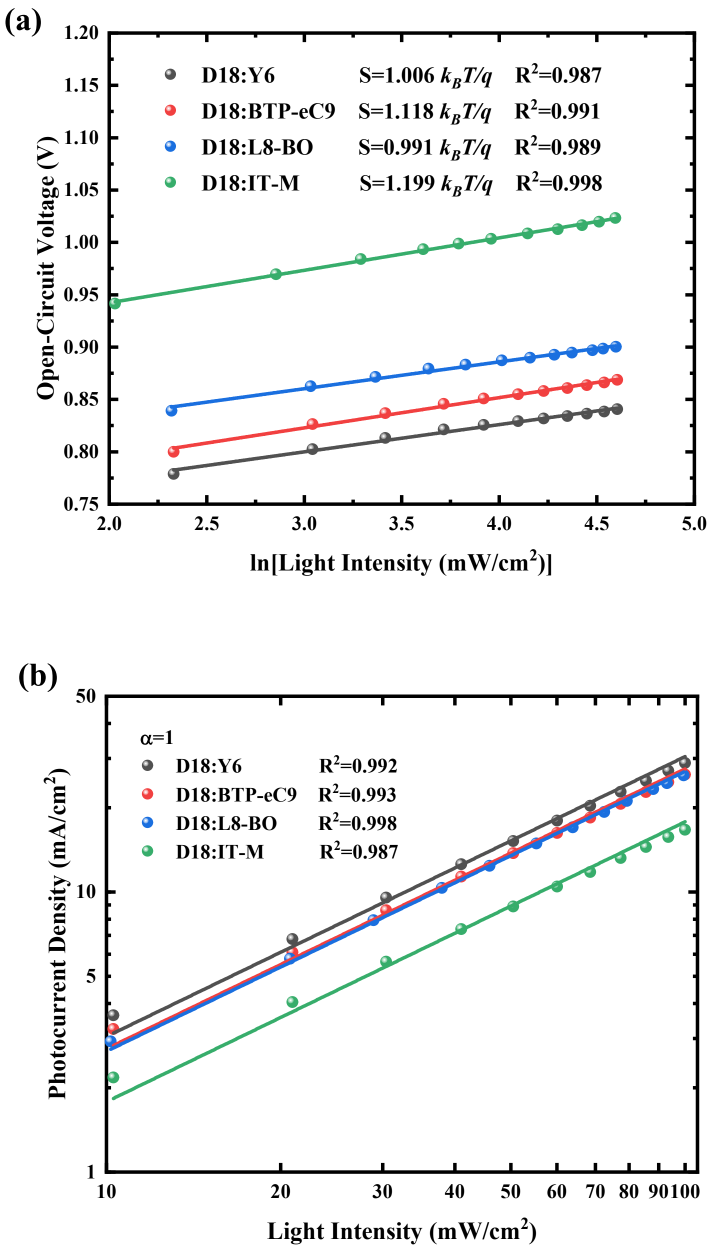

Fig. S5. (a) Measured V_{oc} and (b) J_{sc} at different light intensities for these four devices. It can be seen that all of these four devices exhibit a slope of 1.0 kT/q in the V_{oc} - ln(P_{light}) plot and an exponent of 1 for $J_{sc} \propto P_{light}^{\alpha}$ in J_{sc}-ln(P_{light}) plot, suggesting second-order recombination dominates (here is bimolecular recombination process) in these devices.

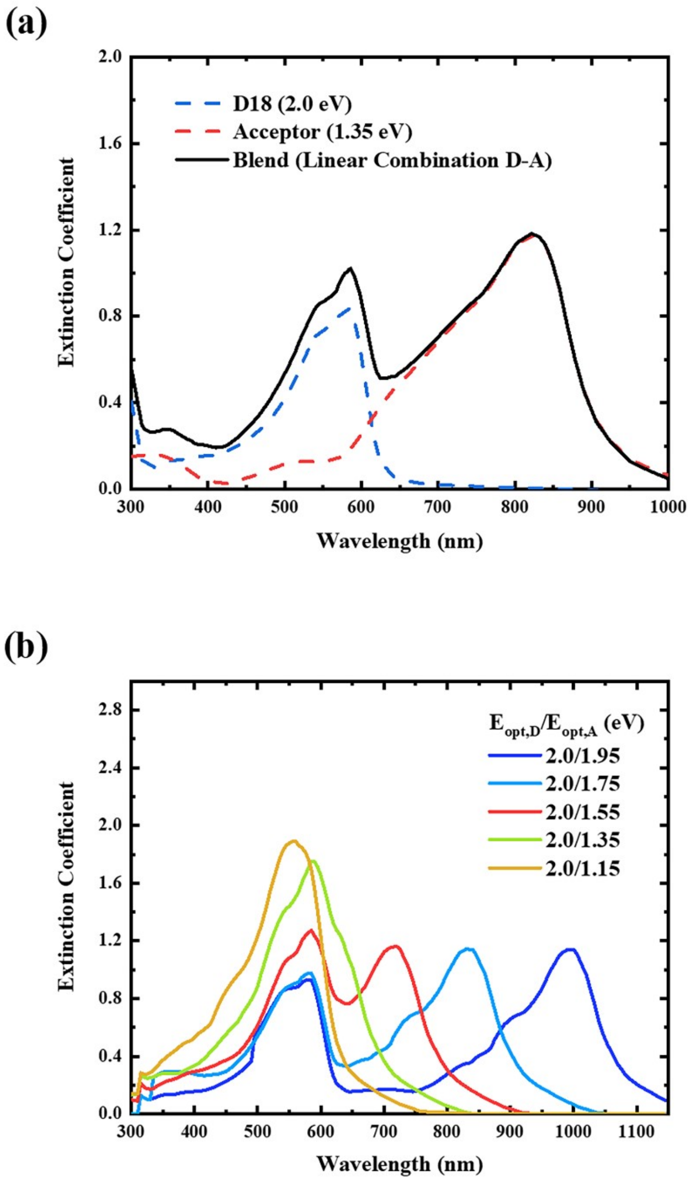

Fig. S6. (a) We assume the extinction coefficient spectrum of the blend (black solid line) is the superposition of polymer donor D18 (blue dotted line) and acceptor Y6 (red dotted line). (b) Make the extinction coefficient curve of L8-BO red-shift or blue-shift to yield a new acceptor spectrum with the band-edge ranging from 640 nm to 1080 nm, which is then superposed with the spectrum of D18 linearly to generate a new extinction coefficient spectrum of blend films with different optics gaps.

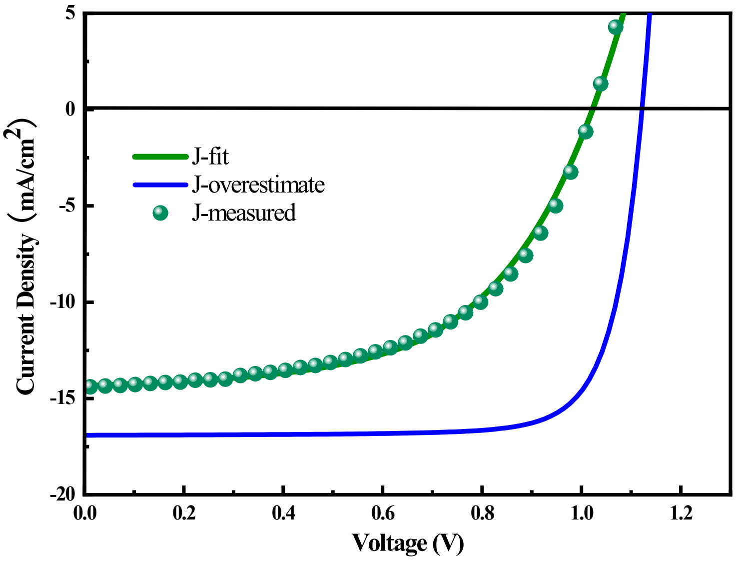

Fig. S7. JV characteristics comparison for D18: IT-M device between experiment and simulation. The green line represents the actual fitting using the measured mobility and other transport parameters as shown in the Table S3. The blue line refers to the situation where assuming the IT-M device share the same mobility, *E*u and Capture rate coefficients as the Y6-series devices as shown in Table S3. It is clearly to see that the Voc and Jsc will be overestimated because of the larger mobility and lower recombination rate coefficient, explaining the error for the point of IT-M device in Fig.4.

Table S1 Summary of E_{gopt} , Voc and $E_{\mathrm{loss.}}$

	E_{gopt} (eV)	Voc (V)	E_{loss} (eV)
D18: Y6	1.352	0.845	0.507
D18: BTP-eC9	1.362	0.869	0.493
D18: L8-BO	1.396	0.899	0.497
D18: IT-M	1.586	1.019	0.567

Table S2 Electron/hole mobility and the corresponding Langevin recombination rate coefficient of the D18-based devices.

Active Layer	D18:Y6	D18:BTP-eC9	D18:L8-BO	D18：IT-M
μ_{e} ($\mathrm{cm^2\,V^{-1}\,s^{-1}}$)	1.53×10^{-4}	1.77×10^{-4}	6.21×10^{-4}	1.85×10^{-4}
μ_{h} ($\mathrm{cm^2\,V^{-1}\,s^{-1}}$)	1.17×10^{-4}	6.03×10^{-4}	5.94×10^{-4}	1.54×10^{-4}
$k_{\mathrm{L}}=q min(\mu_{\mathrm{e}},\mu_{\mathrm{h}})/\varepsilon_{\mathrm{r}}\varepsilon_0$ ($\mathrm{cm^3\,s^{-1}}$)	6.04×10^{-11}	9.14×10^{-11}	3.07×10^{-10}	7.74×10^{-11}
$\zeta=k_{\mathrm{n}}/k_{\mathrm{L}}$	0.023	0.019	0.007	0.09

Table S3. Parameters used for the electrical simulations following the procedure in ref [1], presented in **Figure. 1d** and **Figure. 3a,b** in main text. A multiple trapping drift-diffusion model is used.

Parameters	D18:Y6	D18: BTP-eC9	D18: L8-BO	D18：IT-M	Modeling Fixed
Energy bandgap E_g(eV)	1.352	1.362	1.396	1.55	1.4 or Variable
Electron mobility μ_n ($\times10^{-8}$ m^2 V^{-1} s^{-1})	3	4	5	1.5	3.3 or Variable
Hole mobility μ_p ($\times10^{-8}$ m^2 V^{-1} s^{-1})	3	4	5	1.5	3.3 or Variable
Eff. density of states N_c ($\times10^{26}$ m^{-3})	0.9±0.1			1	1
Generation rate G ($\times10^{28}$ m^{-3} s^{-1})	Optical simulation				
Relative dielectric constant ε_r	3.8				
Urbach energy E_u (meV)	55±1			90	50
DOS per energy interval N_{c0} ($\times10^{25}$ m^{-3} eV^{-1})	5				
Capture rate coefficients b_n ($\times10^{-19}$ m^{-3} s^{-1})	4			7	4
Capture rate coefficients b_p ($\times10^{-19}$ m^{-3} s^{-1})	4			7	4
ΔHOMO-B (eV)	0.15	0.14	0.13	0.04	0.11 or Variable
E_{fn}-E_c (eV)	-0.2				
E_{fp}-E_v (eV)	0.2				
Active layer thickness d (nm)	110				

Table S4 HOMO values of the materials used in this study from literature, measured by UPS.

	HOMO (eV)	Reference
D18	-5.21	[2]
Y6	-5.71	[3]
D18: BTP-eC9	-5.68	[3]
D18: L8-BO	-5.67	[4]
D18: IT-M	-5.58	[5]

3. Supporting Information Note

Supporting Information Note 1

Solving the exciton generation rate $G_{ex}(\lambda, x)$. Following the procedure in ref [6] in main text, the distribution of optical filed $|E(\lambda, x)|$ can be obtained. Combined with absorption coefficient of the photoactive layer blend, *α(λ)*, where λ is the wavelength of the incident light. And $\alpha(\lambda)=4\pi k/\lambda$, where *k* is the extinction coefficient. By assuming a perfect charge generation quantum yield, the charge generation profile for a given wavelength can be described by

$$G_{ex}(\lambda, x) = \frac{1}{2h}\varepsilon_0 \alpha(\lambda)\tilde{n}(\lambda)\lambda\left|E(\lambda, x)\right|^2 \tag{S1}$$

where *h* is the Planck’s constant, ε_0 the vacuum permittivity, and $\tilde{n}$ the real part of the refractive index.

Supporting Information Note 2

Transient Photovoltage (TPV) and Photocurrent (TPC) measurements were carried out following a well-established experimental setup[7]. Charge carriers were generated by a laser pulse excitation at 532 nm, with a pulse width of 8 ns at a frequency of 20 Hz from an Nd: YAG solid nanosecond pulse laser (Q-smart 100 of Quantel). For TPV measurement, the signal was recorded by a Tektronix DPO4014 oscilloscope with 1MΩ input impedance under open-circuit condition. The V_{OC} of the devices were tuned by adjusting the illumination intensity of a 100 W bromine tungsten lamp through the use of neutral density filters, producing steady-state illumination intensity between 10 and 1000 W m^{-2} (corresponding to 0.01–1.0 sun). For TPC measurement, solar cell devices were in series with a 50Ω load resistor and voltage transient across the resistor was recorded by the oscilloscope under the same illumination and laser perturbation. The transient is translated into a current transient by Ohm's law. The photo-generated charge ΔQ by laser perturbation is the time-integrated current transient. All transient data consist of 64 voltage transient averaged together to counteract the fluctuation of laser pulse.

We carried out the transient photovoltage (TPV) and transient photocurrent (TPC) techniques to measure the charge carrier density and together with their lifetime,1 which are the most important parameters to characterize charge carrier recombination dynamics. TPV measurements monitor the transient photovoltage decay generated by a small laser pulse during various constant bias light, enabling us to determine the charge carrier lifetimes corresponding to different open circuit voltages. TPC is measured with identical laser and bias light but under short circuit condition. Combined with TPV, charge carrier density and lifetime can be obtained based on differential charging principle.

The typical OPV devices can be viewed as variable capacitors with various bias light intensity. We can acquire the differential capacitors due to various bias light so as to extract the average charge carrier density in active layer $\bar{n}$ under various bias voltage:

$$\bar{n} = \frac{1}{Adq} \int_{0}^{V_{oc}} \left[C_{\mathrm{DC}}(V) - C_0 \right] dV$$

Noted that the measured capacitance C_{DC} should be subtracted by a geometric capacitance C_0 due to the plate electrode to obtain the differential capacitance C_{diff}. A is the effective cell area, q is the elementary charge and d is the thickness of the active layer. For BHJ, d is the actual thickness of the active layer because the electrons and holes are distributed randomly throughout the active layer. Differential capacitance C_{diff} is much larger than the geometric capacitance.

Supporting Information Note 3

In ref [1] based on the recombination via exponential tail of localized states, the recombination rate via conduction-band state is given by

$$
\begin{aligned}
R_{\mathrm{CBT}} &= \int_{E_V}^{E_C} N_{\mathrm{CBT}}(E_t)\eta_R(E_t)dE_t \\
&= \int_{E_V}^{E_C} N_{\mathrm{C0}} \exp\left(\frac{E_t - E_C}{E_{\mathrm{UC}}}\right) \frac{np - n_i^2}{\left(n + N_C \exp\left[(E_t - E_C)/kT\right]\right)/\beta_p^- + \left(p + N_V \exp\left[(E_V - E_t)/kT\right]\right)/\beta_n^0} dE
\end{aligned}
$$

Hole density p near conduction band can be neglected, so

$$
R_{CBT} = \int_{Ev}^{Ec} N_{c0} \exp(\frac{E_{\mathrm{t}} - E_c}{E_{uc}}) \frac{np\beta_p^-}{N_c \exp\left(\frac{E_{\mathrm{t}} - E_{\mathrm{c}}}{kT}\right)} dE_{\mathrm{t}} = np\beta_p^- \frac{N_{c0}}{N_c} \int_{E_{fn}}^{E_c} \exp(\frac{E_{\mathrm{t}} - E_c}{E_{uc}}) \exp\left(\frac{E_{\mathrm{c}} - E_{\mathrm{t}}}{kT}\right) dE_{\mathrm{t}}
$$

After simple integral operation, we get

$$
R_{CBT} = np\beta_p^- \frac{N_{c0}}{C_0 N_c} \left(1 - \exp(C_0(E_{fn} - E_c))\right)
$$

Where $C_0 = \frac{(kT - E_{uc})}{kT * E_{uc}}$. Similarly, recombination rate via valence-band state R_{VBT} is given by

$$
R_{VBT} = np\beta_p^- \frac{N_{v0}}{D_0 N_v} \left(\exp(D_0(E_{fp} - E_v)) - 1\right)
$$

Where $D_0 = \frac{(E_{uv} - kT)}{kT * E_{uv}}$. And the whole recombination rate R is the sum of both R_{CBT} and R_{VBT}, so

$$
R = R_{CBT} + R_{VBT} = \left[\beta_p^- \frac{N_{c0}}{C_0 N_c} \left(1 - \exp(C_0(E_{fn} - E_c))\right) + \beta_p^- \frac{N_{v0}}{D_0 N_v} \left(\exp(D_0(E_{fp} - E_v)) - 1\right)\right] np
$$

And $R = k_2 np$, if the parameters of both conduction-band and valence band are equal, the k_2 is further simplified as

$$k_2 = \frac{2\beta_{np} N_{c0} V_t * E_u}{(V_t - E_u) * N_c} \left[1 - \exp\left(\frac{V_t - E_u}{V_t * E_u} (E_{fn} - E_c) \right) \right]$$

Supporting Information Note 4

- Prediction model based on varying optical bandgap and energy offset.

First, we take the shape of extinction coefficient spectrum of L8-BO as an example and shift the long-wavelength edge from 640 nm to 1080 nm (corresponding to bandgap between 1.95 eV and 1.05 eV), as Fig. S5 shown. This new spectrum of acceptor is linearly superposed with the one of D18 to obtain a new extinction coefficient spectrum of the blend.

Having generated the composite extinction coefficient of the active layer across the entire visible-NIR spectrum with decreasing energy bandgap but increasing absorption, we can study the optimal bandgap of NFA for the optimal performance based on the D18 donor. Apart from bandgap, we focus on the impact of energy offset which is reflected by $\Delta\mathrm{HOMO}-B$ in Figure 2(a). We set the mobility as 3×10^{-4} $\mathrm{cm^2V^{-1}s^{-1}}$ according to the general measurement results with IQE following Equation (2).

Supporting Information Note 5

We measured the electroluminescence spectra of D18:Y6 and D18:IT-M solar cells at different injection current densities to further elucidate the nonradiative recombination. In order to more clearly distinguish the change of the electroluminescence intensity of the charge-transfer state and the single excited state under different injection currents, the electroluminescence spectra were normalized, as shown in Fig.S6 (b) and S6 (d). For the D18:IT-M solar cell, when the injection current increases, the proportion of the signal from the acceptor single excited state in the electroluminescence spectrum monotonically increases, as shown in Fig. 6(d). This is because after the charge transfer state is filled, the injected excess electrons can only recombine through the higher energy IT-M single excited state energy level. The presented experimental data show no clear charge-transfer state absorption or emission features for D18:Y6 solar cells. When the injection current density increases, there is still only the charge transfer state signal in the electroluminescence spectrum, mainly due to the high intrinsic $\mathrm{EQE}_{\mathrm{EL}}$ of Y6.

Reference

---

1 T. Kirchartz, B. E. Pieters, J. Kirkpatrick, U. Rau and J. Nelson, *Physical Review B*, 2011, **83**, 115209.

2 C. Yang, S. Zhan, Q. Li, Y. Wu, X. Jia, C. Li, K. Liu, S. Qu, Z. Wang and Z. Wang, Nano Energy, 2022, 98, 107299.

3 R. Wang, D. Zhang, X. Zhang and J. Yu, Dyes and Pigments, 2022, 199, 110083.

4 R. Sun, Y. Wu, X. Yang, Y. Gao, Z. Chen, K. Li, J. Qiao, T. Wang, J. Guo, C. Liu, X. Hao, H. Zhu and J. Min, *Adv. Mater.*, 2022, **34**, 2110147.

5 Y. Zhang, D. Liu, T. K. Lau, L. Zhan, D. Shen, P. W. Fong, C. Yan, S. Zhang, X. Lu and C. S. Lee, Adv. Funct. Mater., 2020, 30, 1910466.

6 L. A. A. Pettersson, L. S. Roman and O. Inganäs, *Journal of Applied Physics*, 1999, **86**, 487-496.

7 C. Shuttle, B. O'regan, A. Ballantyne, J. Nelson, D. Bradley, J. De Mello and J. Durrant, *Applied Physics Letters*, 2008, **92**, 80.